

Low temperature phase transitions under CDW state in kagome metals AV_3Sb_5 (A=Cs,Rb,K): Significance of mix-type Fermi surface electron correlations

Huang Jianxin¹, Rina Tazai², Youichi Yamakawa¹, Seiichiro Onari¹, and Hiroshi Kontani¹

¹Department of Physics, Nagoya University, Nagoya 464-8602, Japan

²Yukawa Institute for Theoretical Physics, Kyoto University, Kyoto 606-8502, Japan

(Dated: May 30, 2023)

To understand the multistage phase transitions in V-based kagome metals inside the charge-density-wave (CDW) state, we focus on the impact of the “mix-type” Fermi surface because it is intact in the CDW state on the “pure-type” Fermi surface. On the mix-type Fermi surface, moderate spin correlations develop, and we reveal that uniform ($\mathbf{q} = \mathbf{0}$) bond order is caused by the paramagnon interference mechanism, which is described by the Aslamazov-Larkin vertex correction. The most dominant solution is the E_{2g} -symmetry nematic order, in which the director can be rotated arbitrarily. In addition, we obtain the A_{1g} -symmetry non-nematic order, which leads to the change in the volume. These results are useful to understand the multistage phase transitions inside the 2×2 CDW phase. The present theory has a general significance because mix-type band structure is universally present in kagome lattice tight-binding models.

Introduction.— Exotic electronic states and correlation-driven superconductivity in kagome metals AV_3Sb_5 (A=K, Cs, and Rb) have attracted increasing attention. Strong Coulomb interaction and the geometrical frustration of V site electrons (in Fig. 1 (a)) give rise to exotic quantum phase transition without magnetization. At ambient pressure ($P = 0$), AV_3Sb_5 exhibits 2×2 bond-order (BO) at $T_{\text{BO}} = 78, 94$ and 102 K for A=K, Cs and Rb, respectively [1–5]. The BO is the correlation-driven modulation of the hopping integrals (δt) shown in Fig. 1 (b). The superconducting state appears at $T_c = 1 \sim 3$ K inside the BO phase [6, 7]. Under pressure, T_{BO} gradually decreases, while T_c exhibits non-monotonic pressure dependence [8]. The maximum T_c (~ 10 K) is realized around the BO critical pressure $P_c^{\text{BO}} \approx 2$ GPa, consistently with the BO fluctuation pairing mechanism proposed in Ref. [9]. The predicted s -wave superconductivity has been recently confirmed by the penetration depth and electron irradiation measurements [10, 11].

The nature of rich symmetry-breaking states inside the BO phase has been a significant open problem. For example, the C_6 symmetry-breaking nematic state [12, 13] and the time-reversal-symmetry breaking (TRSB) without spin order [4, 14–18] have been reported. A natural candidate for these states is the correlation-driven hopping integral modulation: δt_{ij} . The nematic order is given by the bond order with real δt_{ij} , and the TRSB order is given by the imaginary δt_{ij} . The latter accompanies topological charge-current [19] that gives the giant anomalous Hall effect (AHE) [20, 21]. Sizable off-site interaction due to beyond-mean-field mechanisms [9, 22–39] may lead to the current order and C_2 coexisting state in kagome metals.

At present, the onset temperatures of symmetry-breaking states inside the BO phase depend on experimental techniques. As for the TRSB state, the TRSB order parameter strongly develops below $T^* = 35 \sim 50$ K

in the μ -SR [14, 16–18] and the AHE [20, 21] measurements, while a small TRSB signal appears just below T_{BO} in many experiments. To understand the difference of T_{TRSB} , the drastic magnetic field (h) effect on the TRSB state due to the h -bond-current trilinear coupling would be important [35]. As for the nematic state, the scanning birefringence study [13] reports $T_{\text{nem}} \approx T_{\text{BO}}$, while $T_{\text{nem}} \approx 35$ K is reported by the elastoresistance measurement [12]. This discrepancy may indicate that the BO layer stacking with π -shift leads to the weak nematicity at T_{BO} , and another nematic order emerges inside the BO phase. The origin of the latter nematicity is not understood at present.

In V-based kagome metals, two major Fermi surfaces (FSs) are composed of the b_{3g} -orbitals and the b_{2g} -orbitals shown in Fig. 1 (a). The bandstructure and the FSs are shown in Figs. 1 (c) and (d), respectively. Both FSs give large density-of-states (DOS) at the Fermi level due to the van-Hove singularity (vHS) at three M points. The b_{3g} -orbital FS is called the “pure-FS”, where each vHS point is composed of a single sublattice; see Fig. 1 (e). The vHS points are gapped by the 2×2 BO on the pure-FS; see Fig. 1 (d). Previous theories have mainly been devoted to understanding the significant roles of the pure-type FS [9, 31–33] except for Refs. [37, 39]. However, one may expect that an additional phase transition below T_{BO} would occur on the mix-type FS because it is not harmed by the BO. Its sublattice weight is shown in Fig. 1 (f). In addition, it is notable that the mix-type band universally exists in usual kagome lattice models. Therefore, the research on the mix-type band is of great significance.

In this paper, to understand the phase transitions below T_{BO} in AV_3Sb_5 , we focus on the impact of the mix-type FS because it is intact in the BO phase. On the mix-type FS, moderate spin correlations develop, and it is revealed that the paramagnon interference mechanism leads to the uniform ($\mathbf{q} = \mathbf{0}$) bond order. This beyond-

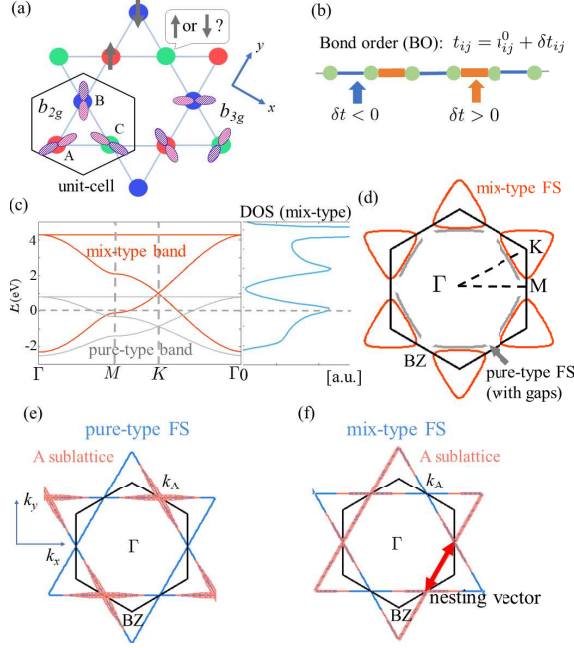


FIG. 1. (a) Kagome lattice structure with geometrical frustration. b_{3g} - and b_{2g} -orbitals are shown. (b) BO parameter given by the hopping integral modulation δt_{ij} . (c) Pure-type (b_{3g} -orbital) and mix-type (b_{2g} -orbital) band structure with vHS points and the DOS. (d) FSs of pure-type FS ($n^{\text{pure}} = 2.6$) and mix-type FS ($n^{\text{mix}} = 1.6$). Here, the pure-type FS exhibits the 2×2 BO induced gap. (e) A-sublattice weight on the pure-type FS at the van-Hove filling $n_{\text{vHFe}}^{\text{pure}} = 2.5$. The vHS point at $\mathbf{k} = \mathbf{k}_A$ is composed of A sublattice. (f) A-sublattice weight on the mix-type FS at the van-Hove filling $n_{\text{vHFe}}^{\text{mix}} = 1.5$. The vHS point at $\mathbf{k} = \mathbf{k}_A$ is composed of B+C sublattices.

mean-field mechanism is described by the Aslamazov-Larkin vertex correction. The most dominant solution is the E_{2g} -symmetry nematic order in which the director can be rotated arbitrarily. In addition, we obtain the A_{1g} -symmetry non-nematic order, which leads to the change in the volume. These results are useful to understand the multistage phase transitions inside the 2×2 BO phase.

Model Hamiltonian and Formulations.— In this paper, we study the quantum phase transition in kagome lattice Hubbard model with a “mix-type” band composed of three b_{2g} orbitals. We apply the density-wave (DW) equation method to derive the optimized order parameter (= symmetry breaking in the self-energy) driven by the beyond-mean-field vertex corrections. In Ref. [9], the present authors studied the $b_{2g}+b_{3g}$ orbital kagome lattice Hubbard model for AV_3Sb_5 , and found that the pure-type FS alone gives the 2×2 BO state. However, the b_{2g} orbital FS can induce different instabilities for $T \ll T_{\text{BO}}$. For this reason, to find the phase transition inside the BO phase, we study the b_{2g} orbital kagome lattice Hubbard model.

The b_{2g} orbitals at sublattices A-C are shown in Fig.

1 (a). The corresponding mix-type FS is shown in Fig. 1 (d). The kinetic term of the b_{2g} orbital model is

$$H_0 = \sum_{\mathbf{k}, l, m, \sigma} h_{lm}(\mathbf{k}) c_{\mathbf{k}, l, \sigma}^\dagger c_{\mathbf{k}, m, \sigma}, \quad (1)$$

where $l, m = \text{A, B, C}$ and σ is the spin index. In our study the unit of energy (Coulomb interaction, hopping integral and temperature) is eV. We set the nearest-neighbor hopping integral $t = -0.5$ [9, 31] and put number of electrons on mix-type band $n^{\text{mix}} = 1.6$. The 3×3 Green function is given as $\hat{G}(\mathbf{k}, \epsilon_n) = ((i\epsilon_n + \mu)\hat{1} - \hat{h}(\mathbf{k}))^{-1}$, where $\epsilon_n = (2n + 1)\pi T$ is the fermion Matsubara frequency.

We also introduce the on-site Coulomb interaction term $H_U = U \sum_{i,l} n_{i,l,\uparrow} n_{i,l,\downarrow}$, where $n_{i,l,\sigma}$ is the electron number at unit cell i . In the mean-field-level approximation, the spin instability is the most prominent [9]. In the random phase approximation (RPA), spin susceptibility is derived from:

$$\hat{\chi}^s(q) = \hat{\chi}^0(q)(\hat{1} - \hat{\Gamma}^s \hat{\chi}^0(q))^{-1}, \quad (2)$$

where $\hat{\chi}^0(q)$ is the 3×3 irreducible susceptibility matrix and $q \equiv (\mathbf{q}, \omega_l = 2\pi Tl)$. The spin susceptibility diverges when the spin Stoner factor α_s , which is defined as the maximum eigenvalue of $U\hat{\chi}^0(q)$, reaches unity. Figure 2 (a) shows the spin susceptibility $\chi_{\text{A,A}}^s(\mathbf{q})$ at $T = 0.02$ and $\alpha_s = 0.97$ ($U = 2.2$). Its maximum peak appears at the nesting of the A-sublattice FS shown in Fig. 1 (f). The real-space short-range spin correlation is depicted in Fig. 2 (b).

Here, we shortly discuss the spin-fluctuation-mediated superconductivity on the mix-type FS [31] by solving the linearized gap equation:

$$\lambda_{\text{SC}} \Delta_{lm}(k) = T \sum_{k' l' m'} V_{lm}^{\text{SC}}(k - k') G_{ll'}(k') G_{mm'}(-k') \times \Delta_{l' m'}(k'), \quad (3)$$

where $V_{lm}^{\text{SC}}(q) = -\frac{3U^2}{2} \chi_{lm}^s(q) + \frac{U^2}{2} \chi_{lm}^c(q)$. Here, λ_{SC} is the eigenvalue of the gap equation, and $\Delta_{lm}(k)$ is the gap function. Figures 2 (c)-(d) are the obtained dominant superconducting gap function for $\alpha_s = 0.97$ ($U = 2.2$) and $T = 0.02$. The obtained largest eigenvalue ($\lambda_{\text{SC}} = 0.72$) corresponds to doubly degenerate d_{xy} - and $d_{x^2-y^2}$ -wave singlet state. The d_{xy} -wave gap function is shown in Fig. 2 (c). In addition, the $f_{y^3-2x^2y}$ -wave triplet state with $\lambda_{\text{SC}} = 0.44$ is obtained. This gap function is shown in Fig. 2 (d). Thus, various unconventional pairing states can be realized on the mix-type FS.

DW equation analysis.— From now on, we study the phase transition based on the DW equation theory. In this theory, various nonmagnetic DW orders are induced by the beyond-RPA non-local correlations, called the vertex corrections. This theory was first developed to explain the orbital nematic state in Fe-based superconductors, and it has been applied to the cuprates and the

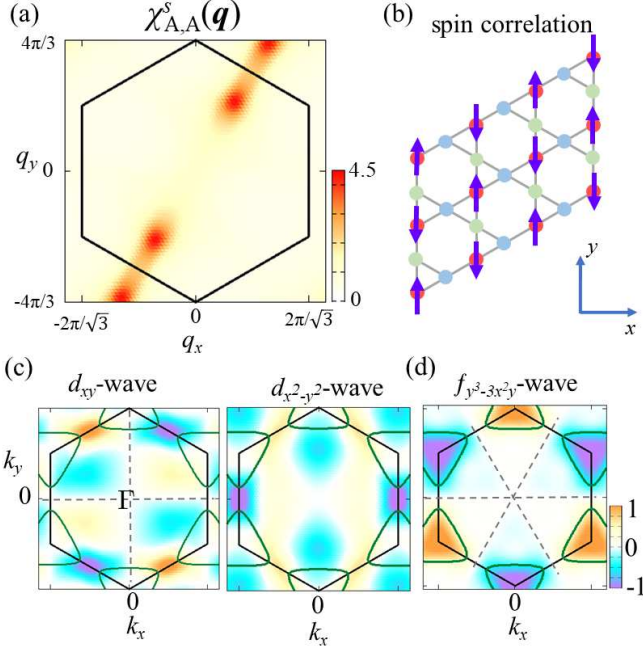


FIG. 2. (a) Spin susceptibility $\chi_{A,A}^s(\mathbf{q})$. Its peak locates on the Brillouin zone. (b) Real-space short-range spin correlation. (c)-(e) Superconducting gap functions given by the gap equation for $\alpha_S = 0.97$ and $T = 0.02$: (c) (d_{xy} , $d_{x^2-y^2}$)-wave singlet gap with $\lambda_{SC} = 0.72$ and (d) f -wave triplet gap with $\lambda_{SC} = 0.44$.

twisted-bilayer graphene successfully [29]. Recently, the BO and current order states in kagome metals with pure-type band have been explained [9, 34]. The DW equation for the charge-channel order is given as

$$\lambda_{\mathbf{q}} f_{\mathbf{q}}^L(k) = -\frac{T}{N} \sum_{p, M_1, M_2} I_{\mathbf{q}}^{L, M_1}(k, p) \times \{G(p)G(p + \mathbf{q})\}^{M_1, M_2} f_{\mathbf{q}}^{M_2}(p), \quad (4)$$

where $I_{\mathbf{q}}^{L, M}(k, p)$ is the “particle-hole (p-h) pairing interaction”, $k \equiv (\mathbf{k}, \epsilon_n)$ and $p \equiv (\mathbf{p}, \epsilon_m)$ (ϵ_n, ϵ_m are fermion Matsubara frequencies). $L \equiv (l, l')$ and $M_i \equiv (m_i, m'_i)$ represent the pair of sublattice indices A, B, C. $\lambda_{\mathbf{q}}$ is the eigenvalue that represents the instability of the DW at wavevector \mathbf{q} , and $\max_{\mathbf{q}} \{\lambda_{\mathbf{q}}\}$ reaches unity at $T = T_{DW}$. $f_{\mathbf{q}}^L(k)$ is the Hermitian form factor that is proportional to the p-h condensation $\sum_{\sigma} \{ \langle c_{\mathbf{k}+\mathbf{q}, l, \sigma}^{\dagger} c_{\mathbf{k}, l', \sigma} \rangle - \langle \cdots \rangle_0 \}$, or equivalently, the symmetry-breaking component in the self-energy. In real space, the \mathbf{k} -dependent form factor gives the correlated hopping between (i, l) and (j, m) , which is given as: $\delta t_{il, jm} (= \delta t_{jm, il})^*$.

$$\delta t_{il, jm} = \frac{1}{N} \sum_{\mathbf{k}} f_{\mathbf{q}}^{lm}(\mathbf{k}) e^{i\mathbf{k} \cdot (\mathbf{r}_{il} - \mathbf{r}_{jm})} e^{i\mathbf{q} \cdot \mathbf{r}_{il}}, \quad (5)$$

where \mathbf{r}_{il} represents position of l sublattice in the unit-cell i . The BO preserves the time-reversal-symmetry: $\delta t_{il, jm} = \delta t_{jm, il} = \text{real}$.

The kernel function $I_{\mathbf{q}}^{L, M}$ in the DW equation is given by the functional derivative of the Luttinger ward function $\Phi_{LW}(G)$. Here, we apply the fluctuation-exchange approximation for $\Phi_{LW}(G)$. Then, $I_{\mathbf{q}}^{L, M}$ is composed of one Hartree term, one single-magnon exchange Mak-Thompson (MT) term and two double-magnon interference Aslamazov-Larkin (AL) terms, as depicted in Fig. 3 (a) [29]. Importantly, the AL terms represent the “interference between two paramagnons with momenta \mathbf{Q} and \mathbf{Q}' ” that leads to the DW order at $\mathbf{q} = \mathbf{Q} - \mathbf{Q}'$; see Fig. 3 (b).

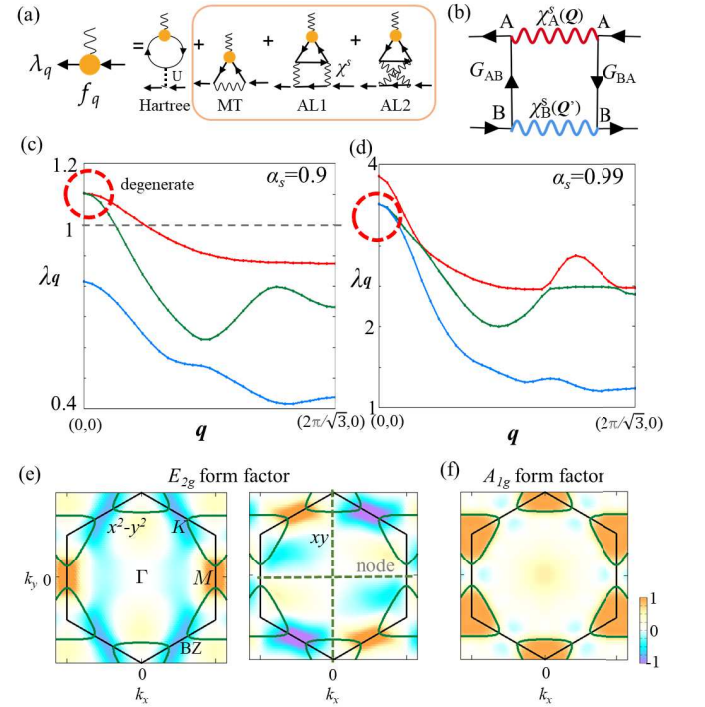


FIG. 3. (a) Linearized DW equation with respect to the form factor $f_{\mathbf{q}}(k)$ and eigenvalue $\lambda_{\mathbf{q}}$. The p-h pairing interaction is composed of the Hartree term, the MT term, and the AL terms. (b) Interference between two paramagnons (\mathbf{Q} and \mathbf{Q}') that leads to the DW order at $\mathbf{q} = \mathbf{Q} - \mathbf{Q}'$. (c-d) Eigenvalue $\lambda_{\mathbf{q}}$ for two cases: (c) Moderate spin fluctuation case with $\alpha_S = 0.9$ and (d) strong spin fluctuation case with $\alpha_S = 0.99$. The first, second, and third eigenvalues are shown in different colors. In both cases, $\lambda_{\mathbf{q}}$ exhibits the maximum at $\mathbf{q} = \mathbf{0}$. (e-f) Diagonal form factor $\sum_{l}^{A, B, C} f_{\mathbf{q}}^{ll}(k)$: (e) E_{2g} symmetry solution obtained for $\alpha_S = 0.9$ and (f) A_{1g} symmetry solution obtained for $\alpha_S = 0.99$. Note that off-diagonal form factor is also large.

With the obtained spin susceptibility, we solve the DW equation. The \mathbf{q} -dependence of the eigenvalue $\lambda_{\mathbf{q}}$ at $n^{\text{mix}} = 1.6$ ($T = 0.02$) is exhibited in Figs. 3 (c) and (d). (Here, we show $\lambda_{\mathbf{q}}$ only on the path Γ - M because $\lambda_{\mathbf{q}}$ on the path M - K - Γ is small.) Figure 3 (c) [(d)] shows the result for $\alpha_S = 0.9$ (0.99), where spin fluctuation strength is moderate [strong]. Importantly, the maximum peak position is located at $\mathbf{q} = \mathbf{0}$ in both

cases. The obtained $\mathbf{q} = \mathbf{0}$ order, which is very different from the nesting driven $\mathbf{q} \neq \mathbf{0}$ order, is naturally derived from the interference between two paramagnons with wavevectors \mathbf{Q} and $-\mathbf{Q}'$ [29]. For $\alpha_S = 0.9$ in Fig. 3 (c), the largest eigenvalues are degenerate, and the corresponding form factors are E_{2g} symmetry BO; ($\hat{f}_{x^2-y^2}(k)$, $\hat{f}_{xy}(k)$). Diagonal form factor $\sum_l f^{ll}(k)$ is shown in Fig. 3 (e). Note that off-diagonal form factors are as large as the diagonal form factors. For $\alpha_S = 0.99$ in Fig. 3 (d), the non-degenerate largest eigenvalue corresponds to A_{1g} symmetry form factor shown in Fig. 3 (f).

The E_{2g} symmetry BO gives the nematicity, and its director can be rotated at any angle by taking the linear combination of $\hat{f}_{x^2-y^2}(k)$ and $\hat{f}_{xy}(k)$ [24]. To understand the nature of the E_{2g} symmetry nematic state, we discuss the real-space form factor $\delta t_{il,jm}$ based on Eq. (5). When the wavevector is $\mathbf{q} = \mathbf{0}$, $\delta t_{il,jm}$ is simply written as $\delta t_{lm}(\mathbf{r})$ with $\mathbf{r} \equiv \mathbf{r}_{il} - \mathbf{r}_{jm}$. The obtained $\delta t_{lm}(\mathbf{r})$ for $f_{x^2-y^2}^{lm}(k)$ at $\mathbf{q} = \mathbf{0}$ is shown in Fig. 4 (a). (Its schematic picture is given in Fig. 4 (b).) It is plotted in three directions (AB, AC and BC) from sublattice A or B, as a function of the distance R , where the distance between nearest sites is 1. (The even-parity relation $\delta t_{lm}(R) = \delta t_{ml}(-R)$ is verified.) δt_{ll} at $R = 0$ represents the onsite charge modulation at sublattice l , and δt_{lm} at $R = \pm 1$ ($l \neq m$) represents BO between the nearest sites.

A schematic picture of the hopping modulation due to the nearest BO is given in Fig. 4 (c). In this case, the lattice structure will become nematic in the presence of finite electron-phonon coupling due to E_{2g} acoustic mode. We also discuss the FS deformation due to the E_{2g} nematic BO, under the order parameter $H' = \Delta E \sum_{\mathbf{k}\sigma} \hat{c}_{\mathbf{k}\sigma}^\dagger \hat{f}_\theta(\mathbf{k}) \hat{c}_{\mathbf{k}\sigma}$, where $\hat{f}_\theta(\mathbf{k}) \equiv \cos \theta \hat{f}_{x^2-y^2}(\mathbf{k}) + \sin \theta \hat{f}_{xy}(\mathbf{k})$. The ordered nematic FS at $\theta = 0$ with $\delta E = 0.01$ is showed in Fig. 4 (d). By changing the angle θ , the nematic FS can be rotated to any direction. However, the continuous degeneracy with respect to θ will be lifted by the 6th order Ginzburg-Landau free energy terms.

Figure 4 (e) shows the T -dependence of λ for E_{2g} and A_{1g} states, in the case of $U = 1.95$. The obtained λ monotonically increases with decreasing T , while the increment of α_S is moderate (see Fig. 4 (f)). Although the obtained transition temperature is relatively high, it will be reduced to below T_{BO} by introducing the self-energy effect [41].

In the SM A [40], we discuss the important roles of the AL and MT vertex corrections for the nematic order. We find that the largest eigenvalue state changes from E_{2g} BO to A_{1g} BO at $\alpha_s \sim 0.975$. (Simple charge order is prohibited by the Hartree term.) For both even-parity BOs, the AL term gives large positive contribution. In fact, the AL term can stabilize general even-parity BOs, whose wavevector $\mathbf{q} = \mathbf{Q} - \mathbf{Q}'$ (see Fig. 3 (b)) becomes

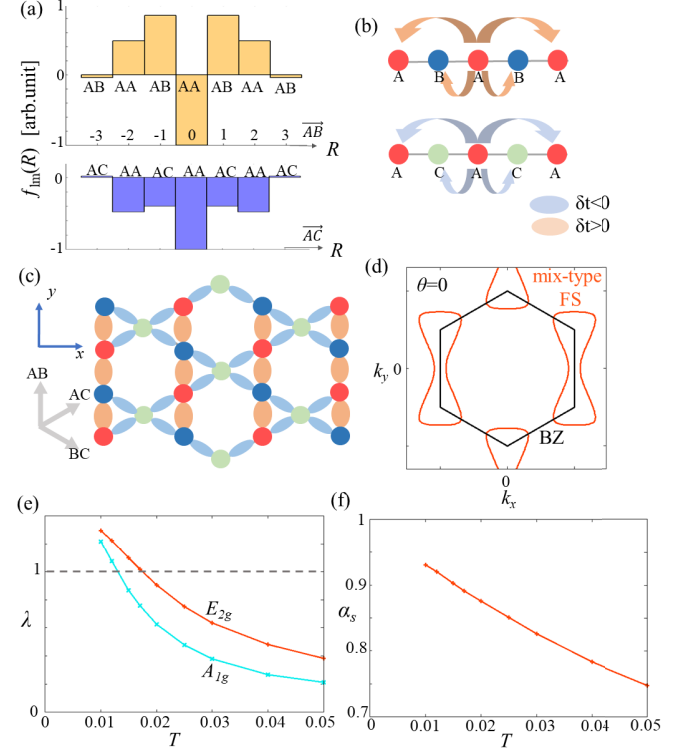


FIG. 4. (a) Real space form factors $\delta t_{lm}(R)$ in three directions. The horizontal axis means the real space distance. For example, in AB direction, $R = 1$ (2) marks the hopping modulation between the nearest A and B (A and A). Note that $\delta t_{AC}(R) = \delta t_{BC}(R)$. (b) Schematic pictures of $\delta t_{lm}(R)$. (c) Nematic bond order in real space for $f_{x^2-y^2}$. Orange means stronger hopping ($\delta t_{ij} > 0$) while blue means weaker one ($\delta t_{ij} < 0$). (d) Nematic FS induced by the nematic BO f_θ . It can be rotated to any angle by changing the angle θ . (e) T -dependence of $\lambda_{q=0}$ for E_{2g} and A_{1g} states, in the case of $U = 1.95$. (f) T -dependence of α_S .

zero or small (minor) nesting vector [29]. In addition, the MT term slightly favors the nodal A_{1g} BO. The A_{1g} BO with $\lambda_{q=0} \sim 2$ will be realized if the self-energy effect reduces the eigenvalue by 50% [29].

The quantum interference mechanism produces the nearest site BO in both the mix-type band and the pure-type band. However, the wavevector is $\mathbf{q} = \mathbf{0}$ in the mix-type band and $\mathbf{q} \neq \mathbf{0}$ in the pure-type band. To understand this difference, we focus on the significant role of the vHS points. Since the vHS is composed of two sublattices in the mix-type band, the $\mathbf{q} = \mathbf{0}$ nearest site BO is efficiently realized by the intra-vHS scattering. In contrast, in the pure-type band, the vHS is composed of a single sublattice. So the inter-vHS gives the inter-site BO at $\mathbf{q} = \mathbf{q}_{\text{vHS}_1} - \mathbf{q}_{\text{vHS}_2}$. Thus, we can understand the different BOs between both bands by using the unique present theory.

Summary. — We studied the phase transitions below T_{BO} in AV_3Sb_5 by focusing on the mix-type FS that is

intact in the BO phase. On the mix-type FS, moderate spin correlations develop, and it is revealed that the paramagnon interference mechanism leads to the uniform ($\mathbf{q} = \mathbf{0}$) bond order. The most dominant solution is the E_{2g} -symmetry nematic order. We also obtain the A_{1g} -symmetry non-nematic order. These results are useful to understand the multistage phase transitions inside the 2×2 BO phase. The present theory has a general significance because mix-type bandstructure is universally present in general kagome lattice models.

This study has been supported by Grants-in-Aid for Scientific Research from MEXT of Japan (JP18H01175, JP20K03858, JP20K22328, JP22K14003, JP23K03299), and by the Quantum Liquid Crystal No. JP19H05825 KAKENHI on Innovative Areas from JSPS of Japan.

[1] B. R. Ortiz, L. C. Gomes, J. R. Morey, M. Winiarski, M. Bordelon, J. S. Mangum, I. W. H. Oswald, J. A. Rodriguez-Rivera, J. R. Neilson, S. D. Wilson, E. Ertekin, T. M. McQueen, and E. S. Toberer, *New kagome prototype materials: discovery of KV_3Sb_5 , RbV_3Sb_5 , and CsV_3Sb_5* , Phys. Rev. Materials **3**, 094407 (2019).

[2] B. R. Ortiz, S. M. L. Teicher, Y. Hu, J. L. Zuo, P. M. Sarte, E. C. Schueller, A. M. M. Abeykoon, M. J. Krogstad, S. Rosenkranz, R. Osborn, R. Seshadri, L. Balents, J. He, and S. D. Wilson, *CsV_3Sb_5 : A \mathbb{Z}_2 Topological Kagome Metal with a Superconducting Ground State*, Phys. Rev. Lett. **125**, 247002 (2020).

[3] C. Mu, Q. Yin, Z. Tu, C. Gong, H. Lei, Z. Li, and J. Luo, *S -Wave Superconductivity in Kagome Metal CsV_3Sb_5 Revealed by $^{121/123}Sb$ NQR and ^{51}V NMR Measurements*, Chin. Phys. Lett. **38**, 077402 (2021).

[4] Y.-X. Jiang, J.-X. Yin, M. M. Denner, N. Shumiya, B. R. Ortiz, G. Xu, Z. Guguchia, J. He, M. S. Hossain, X. Liu, J. Ruff, L. Kautzsch, S. S. Zhang, G. Chang, I. Belopolski, Q. Zhang, T. A. Cochran, D. Multer, M. Litskevich, Z.-J. Cheng, X. P. Yang, Z. Wang, R. Thomale, T. Neupert, S. D. Wilson, and M. Z. Hasan, *Unconventional chiral charge order in kagome superconductor KV_3Sb_5* , Nat. Mater. **20**, 1353–1357 (2021).

[5] H. Li, H. Zhao, B. R. Ortiz, T. Park, M. Ye, L. Balents, Z. Wang, S. D. Wilson, and I. Zeljkovic, *Rotation symmetry breaking in the normal state of a kagome superconductor KV_3Sb_5* , Nat. Phys. **18**, 265–270 (2022).

[6] B. R. Ortiz, P. M. Sarte, E. M. Kenney, M. J. Graf, S. M. L. Teicher, R. Seshadri, and S. D. Wilson, *Superconductivity in the \mathbb{Z}_2 kagome metal KV_3Sb_5* , Phys. Rev. Materials **5**, 034801 (2021).

[7] Q. Yin, Z. Tu, C. Gong, Y. Fu, S. Yan, and H. Lei, *Superconductivity and Normal-State Properties of Kagome Metal RbV_3Sb_5 Single Crystals*, Chin. Phys. Lett. **38**, 037403 (2021).

[8] F. H. Yu, D. H. Ma, W. Z. Zhuo, S. Q. Liu, X. K. Wen, B. Lei, J. J. Ying, and X. H. Chen, *Unusual competition of superconductivity and charge-density-wave state in a compressed topological kagome metal*, Nat. Commun. **12**, 2645 (2021).

[9] R. Tazai, Y. Yamakawa, S. Onari, and H. Kontani, *Mechanism of exotic density-wave and beyond-Migdal unconventional superconductivity in kagome metal AV_3Sb_5 ($A = K, Rb, Cs$)*, Sci. Adv. **8**, eabl4108 (2022).

[10] M. Ropponi, K. Ishihara, Y. Tanaka, K. Ogawa, K. Okada, S. Liu, K. Mukasa, Y. Mizukami, Y. Uwatoko, R. Grasset, M. Konczykowski, B. R. Ortiz, S. D. Wilson, K. Hashimoto, and T. Shibauchi, *Bulk evidence of anisotropic s -wave pairing with no sign change in the kagome superconductor CsV_3Sb_5* , Nat. Commun. **14**, 667 (2023).

[11] W. Zhang, X. Liu, L. Wang, C. W. Tsang, Z. Wang, S. T. Lam, W. Wang, J. Xie, X. Zhou, Y. Zhao, S. Wang, J. Tallon, K. T. Lai, and S. K. Goh, *Nodeless superconductivity in kagome metal CsV_3Sb_5 with and without time reversal symmetry breaking*, Nano Lett. **23**, 872 (2023).

[12] L. Nie, K. Sun, W. Ma, D. Song, L. Zheng, Z. Liang, P. Wu, F. Yu, J. Li, M. Shan, D. Zhao, S. Li, B. Kang, Z. Wu, Y. Zhou, K. Liu, Z. Xiang, J. Ying, Z. Wang, T. Wu, and X. Chen, *Charge-density-wave-driven electronic nematicity in a kagome superconductor*, Nature **604**, 59–64 (2022).

[13] Y. Xu, Z. Ni, Y. Liu, B. R. Ortiz, Q. Deng, S. D. Wilson, B. Yan, L. Balents, and L. Wu, *Three-state nematicity and magneto-optical Kerr effect in the charge density waves in kagome superconductors*, Nat. Phys. **18**, 1470 (2022).

[14] L. Yu, C. Wang, Y. Zhang, M. Sander, S. Ni, Z. Lu, S. Ma, Z. Wang, Z. Zhao, H. Chen, K. Jiang, Y. Zhang, H. Yang, F. Zhou, X. Dong, S. L. Johnson, M. J. Graf, J. Hu, H.-J. Gao, and Z. Zhao, *Evidence of a hidden flux phase in the topological kagome metal CsV_3Sb_5* , arXiv:2107.10714

[15] C. Mielke, D. Das, J.-X. Yin, H. Liu, R. Gupta, Y.-X. Jiang, M. Medarde, X. Wu, H. C. Lei, J. Chang, P. Dai, Q. Si, H. Miao, R. Thomale, T. Neupert, Y. Shi, R. Khasanov, M. Z. Hasan, H. Luetkens, and Z. Guguchia, *Time-reversal symmetry-breaking charge order in a kagome superconductor*, Nature **602**, 245–250 (2022).

[16] R. Khasanov, D. Das, R. Gupta, C. Mielke, M. Elender, Q. Yin, Z. Tu, C. Gong, H. Lei, E. T. Ritz, R. M. Fernandes, T. Birol, Z. Guguchia, and H. Luetkens, *Time-reversal symmetry broken by charge order in CsV_3Sb_5* , Phys. Rev. Research **4**, 023244 (2022).

[17] Z. Guguchia, C. Mielke, D. Das, R. Gupta, J.-X. Yin, H. Liu, Q. Yin, M. H. Christensen, Z. Tu, C. Gong, N. Shumiya, M. S. Hossain, T. Gamsakhurdashvili, M. Elender, P. Dai, A. Amato, Y. Shi, H. C. Lei, R. M. Fernandes, M. Z. Hasan, H. Luetkens, and R. Khasanov, *Tunable unconventional kagome superconductivity in charge ordered RbV_3Sb_5 and KV_3Sb_5* , Nat. Commun. **14**, 153 (2023).

[18] C. Guo, C. Putzke, S. Konyzheva, X. Huang, M. Gutierrez-Amigo, I. Errea, D. Chen, M. G. Vergniory, C. Felser, M. H. Fischer, T. Neupert, and P. J. W. Moll, *Switchable chiral transport in charge-ordered kagome metal CsV_3Sb_5* , Nature **611**, 461–466 (2022).

[19] F. D. M. Haldane, *Model for a Quantum Hall Effect without Landau Levels: Condensed-Matter Realization of the "Parity Anomaly"*, Phys. Rev. Lett. **61**, 2015 (1988).

[20] S.-Y. Yang, Y. Wang, B. R. Ortiz, D. Liu, J. Gayles, E. Derunova, R. Gonzalez-Hernandez, L. Šmejkal, Y. Chen, S. S. P. Parkin, S. D. Wilson, E. S. Toberer, T. McQueen, and M. N. Ali, *Giant, unconventional anomalous Hall effect in the metallic frustrated magnet candidate, KV_3Sb_5* , Sci. Adv. **6**, eabb6003 (2020).

[21] F. H. Yu, T. Wu, Z. Y. Wang, B. Lei, W. Z. Zhuo, J. J. Ying, and X. H. Chen, *Concurrence of anomalous Hall effect and charge density wave in a superconducting topo-*

logical kagome metal, Phys. Rev. B **104**, L041103 (2021).

[22] S. Onari and H. Kontani, *Self-consistent Vertex Correction Analysis for Iron-based Superconductors: Mechanism of Coulomb Interaction-Driven Orbital Fluctuations*, Phys. Rev. Lett. **109**, 137001 (2012).

[23] Y. Yamakawa, S. Onari, and H. Kontani, *Nematicity and Magnetism in FeSe and Other Families of Fe-Based Superconductors*, Phys. Rev. X **6**, 021032 (2016).

[24] S. Onari and H. Kontani, *SU(4) Valley + Spin Fluctuation Interference Mechanism for Nematic Order in Magic-Angle Twisted Bilayer Graphene: The Impact of Vertex Corrections*, Phys. Rev. Lett. **128**, 066401 (2022).

[25] M. Tsuchiizu, Y. Ohno, S. Onari, and H. Kontani, *Orbital Nematic Instability in the Two-Orbital Hubbard Model: Renormalization-Group + Constrained RPA Analysis*, Phys. Rev. Lett. **111**, 057003 (2013).

[26] M. Tsuchiizu, K. Kawaguchi, Y. Yamakawa, and H. Kontani, *Multistage electronic nematic transitions in cuprate superconductors: A functional-renormalization-group analysis*, Phys. Rev. B **97**, 165131 (2018).

[27] A. V. Chubukov, M. Khodas, and R. M. Fernandes, *Magnetism, Superconductivity, and Spontaneous Orbital Order in Iron-Based Superconductors: Which Comes First and Why?*, Phys. Rev. X **6**, 041045 (2016).

[28] R. M. Fernandes, P. P. Orth, and J. Schmalian, *Intertwined Vestigial Order in Quantum Materials: Nematicity and Beyond*, Annu. Rev. Condens. Matter Phys. **10**, 133 (2019).

[29] H. Kontani, R. Tazai, Y. Yamakawa, and S. Onari, *Unconventional density waves and superconductivities in Fe-based superconductors and other strongly correlated electron systems*, Adv. Phys. **70**, 355 (2023).

[30] J. C. S. Davis and D.-H. Lee, *Concepts relating magnetic interactions, intertwined electronic orders, and strongly correlated superconductivity*, Proc. Natl. Acad. Sci. U.S.A. **110**, 17623 (2013).

[31] X. Wu, T. Schwemmer, T. Müller, A. Consiglio, G. Sangiovanni, D. Di Sante, Y. Iqbal, W. Hanke, A. P. Schnyder, M. M. Denner, M. H. Fischer, T. Neupert, and R. Thomale, *Nature of Unconventional Pairing in the Kagome Superconductors AV_3Sb_5 ($A = K, Rb, Cs$)*, Phys. Rev. Lett. **127**, 177001 (2021).

[32] M. M. Denner, R. Thomale, and T. Neupert, *Analysis of Charge Order in the Kagome Metal AV_3Sb_5 ($A = K, Rb, Cs$)*, Phys. Rev. Lett. **127**, 217601 (2021).

[33] T. Park, M. Ye, and L. Balents, *Electronic instabilities of kagome metals: Saddle points and Landau theory*, Phys. Rev. B **104**, 035142 (2021).

[34] R. Tazai, Y. Yamakawa and H. Kontani, *Charge-loop current order and Z3 nematicity mediated by bond-order fluctuations in kagome metal AV_3Sb_5 ($A = Cs, Rb, K$)*, arXiv:2207.08068

[35] R. Tazai, Y. Yamakawa and H. Kontani, *Drastic magnetic-field-induced chiral current order and emergent current-bond-field interplay in kagome metal AV_3Sb_5 ($A = Cs, Rb, K$)*, arXiv:2303.00623

[36] T. Schwemmer, H. Hohmann, M. Durrnagel, J. Potten, J. Beyer, S. Rachel, Y.-M. Wu, S. Raghu, T. Müller, W. Hanke, R. Thomale, *Pair Density Wave Instability in the Kagome Hubbard Model*, arXiv:2302.08517

[37] M. H. Christensen, T. Biro, B. M. Andersen, and R. M. Fernandes, *Loop currents in AV_3Sb_5 kagome metals: Multipolar and toroidal magnetic orders*, Phys. Rev. B **106**, 144504 (2022)

[38] F. Grandi, A. Consiglio, M. A. Sentef, R. Thomale, and D. M. Kennes, *Theory of nematic charge orders in kagome metals*, Phys. Rev. B **107**, 155131 (2023)

[39] H. D. Scammell, J. Ingham, T. Li, and O. P. Sushkov, *Chiral excitonic order from twofold van Hove singularities in kagome metals*, Nat. Commun. **14**, 605 (2023)

[40] Supplementary Materials.

[41] R. Tazai, S. Matsubara, Y. Yamakawa, S. Onari, and H. Kontani, *Rigorous formalism for unconventional symmetry breaking in Fermi liquid theory and its application to nematicity in FeSe*, Phys. Rev. B **107**, 035137 (2023).

[Supplementary Materials]

Huang, Jianxin¹, Rina Tazai², Youichi Yamakawa¹, Seiichiro Onari¹, and Hiroshi Kontani¹

¹Department of Physics, Nagoya University, Nagoya 464-8602, Japan

²Yukawa Institute for Theoretical Physics, Kyoto University, Kyoto 606-8502, Japan

A: Important Roles of the AL and MT Vertex Corrections

Here, we discuss the important roles of the AL and MT vertex corrections for the nematic order. Figure S1 (a) shows the obtained $\lambda_{\mathbf{q}=0}$ for the E_{2g} solution and that for the A_{1g} solution as functions of α_s for $T = 0.02$. These eigenvalues reach unity for $\alpha_s \sim 0.9$. With increasing α_s , the largest eigenvalue state changes from E_{2g} BO to A_{1g} BO at $\alpha_s \sim 0.975$. (Simple charge order is prohibited by the Hartree term.) Figures S1 (b) and (c) give the eigenvalue contributed from the AL and MT terms for the fixed form factor, $\lambda_{\mathbf{q}}^{\text{AL}}$ and $\lambda_{\mathbf{q}}^{\text{MT}}$, respectively. (Note that $\lambda_{\mathbf{q}} = \lambda_{\mathbf{q}}^{\text{AL}} + \lambda_{\mathbf{q}}^{\text{MT}}$.) For both E_{2g} and A_{1g} channels, the AL term gives large positive contribution. In fact, the AL term can stabilize general even-parity BOs, whose wavevector $\mathbf{q} = \mathbf{Q} - \mathbf{Q}'$ (see Fig. 3 (b) in the main text) becomes zero or small (minor) nesting vector [1]. The AL processes give the relation $\lambda_{E_{2g}}^{\text{AL}} \gtrsim \lambda_{A_{1g}}^{\text{AL}}$; see Fig. S1 (b). Thus, the nodal A_{1g} BO originates from the large MT term; see Fig. S1 (c). The A_{1g} BO with $\lambda_{\mathbf{q}=0} \sim 2$ will be realized if the self-energy effect reduces the eigenvalue by 50% [1].

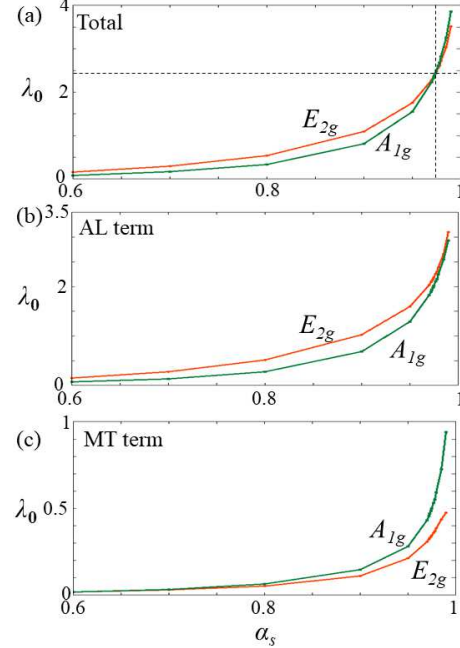


FIG. S1. (a) $\lambda_{\mathbf{q}=0}$ for the E_{2g} solution and that for the A_{1g} solution as functions of α_s for $T = 0.02$. These eigenvalues reach unity for $\alpha_s \sim 0.9$. With $\alpha_s \lesssim 0.975$, the E_{2g} solution has the largest λ . For $\alpha_s \gtrsim 0.975$, it is replaced with the A_{1g} solution. (b)(c) Eigenvalue contributed from the AL and MT terms, $\lambda_{\mathbf{q}}^{\text{AL}}$ and $\lambda_{\mathbf{q}}^{\text{MT}}$, respectively. (Note that $\lambda_{\mathbf{q}} = \lambda_{\mathbf{q}}^{\text{AL}} + \lambda_{\mathbf{q}}^{\text{MT}}$.) While the AL term gives the dominant contribution to $\lambda_{\mathbf{q}=0}$, the MT term plays an important role in determining the symmetry and nodal structure of the form factor.

[1] H. Kontani, R. Tazai, Y. Yamakawa, and S. Onari, *Unconventional density waves and superconductivities in Fe-based superconductors and other strongly correlated electron systems*, arXiv:2209.00539